AIMS Materials Science, 10(4): 710–724.
DOI: 10.3934/matersci.2023039
Received: 11 March 2023
Revised: 17 July 2023
Accepted: 27 July 2023
Published: 21 August 2023

http://www.aimspress.com/journal/Materials

Research article

A study of doped polycrystalline diamond plates by non-destructive methods

Itsh'ak Azoulay[1], Ory Klonsky[2], Yaniv Gelbstein[2,*] and Peter Beker[1,*]

[1] Department of Electrical and Electronics Engineering, Shamoon College of Engineering, Ashdod, 77245, Israel
[2] Department of Materials Engineering, Ben-Gurion University of the Negev, Beer-Sheva 84105, Israel

*** Correspondence:** Email: bakap@sce.ac.il, yanivge@bgu.ac.il; Tel: +972-52-6536364.

Abstract: Diamond offers great promise as a solution to some of the limitations of current state of the art semiconductor technologies. Yet, significant challenges associated with the doping process remain a primary impediment to the development of diamond-based electronic devices. At present, it is unclear which simple measurement methods are needed to evaluate the diamond doping process. We propose non-destructive inspection methods for evaluating the polycrystalline chemical vapor deposition (CVD) diamond doping process, by analyzing the wettability, optical absorption, photoluminescence emission spectroscopy and atmospheric scanning electron microscope (Air-SEM) tests. Our results show that the properties of the measured samples are distinctly changed due to the presence of the doping elements, thereby confirming the effectiveness of these non-destructive methods for the diamond production industry.

K**eywords:** wettability; optical absorption; doping; photoluminescence; Air-SEM

1. Introduction

Diamond exhibits outstanding properties that make it a material of great interest for the semiconductors industry. The industry requires a silicon alternative, that can enable the devices to be smaller, cooler, faster and more powerful. Diamond, as a wide-band semiconductor (5.45 eV), can provide an attractive alternative. Diamond exhibits superior properties, such as: excellent thermal

conductivity, high voltage break down point and fast electron-hole mobility [1,2]. However, the intrinsic carrier concentration of diamond is very poor and the resistivity of pure diamond can exceed 10^{16} Ω·cm (at room temperature) [2]. Therefore, diamond is a semiconductor that must be incorporated with extrinsic dopants, such as nitrogen, phosphorus and boron, in order to reduce the electrical resistivity. With the advent of diamond doping processes [3], the metrological process needs to include an understanding of the diamond doped properties and the possible sources of real time production errors. Diamond metrology challenges include the measurement of surface properties, defect density, homogeneity and composition.

Wettability is a surface property that depends on solid/liquid surface tension and is a very useful tool for getting information about the influence of doping on surface energy. According to wettability theory, solids with high surface tension values should cause high liquid spreading, while solids with low surface tension should cause low liquid spreading. The water contact angle (WCA) is a surface property, and is the basis of a very useful technique for estimating the solid surface tension properties.

Currently, there is a lack of simple and reliable methodologies for simultaneous investigation of relationships between the nature of diamond doped materials and wettability properties. According to the literature, diamond solids have high surface tension values that should cause high water spreading [4]. However, when a bulk of diamond is doped, the WCA can be influenced by the doping materials [5]. Several factors can influence the wettability of diamond materials, including the thickness of the diamond layers, crystal defects, chemical modification, doping, electron affinity and surface roughness [5–7].

The scanning electron microscope (SEM) is a tool commonly used for obtaining nanometer spatial resolution images of the topography, chemistry and dopants mapping [8–10]. Electron microscopy is a favored alternative among the available dopant profiling tools. Two-dimensional dopant profiling is an essential analytic method in semiconductor fabrication. Electron microscopy settings, however, occur at normal vacuum conditions in a vacuum specimen chamber or in gaseous environment specimen chamber environmental scanning electron microscope (ESEM), and limit the size of samples [11,12]. Contactless, non-destructive methods that do not require special treatments for unlimited sized samples are therefore required.

Air-SEM is a scanning electron microscope system that operates at ambient conditions and is capable of measuring insulated, non-coated samples without any size limitation [13]. The atmospheric environment dissipates charge that builds up on the specimen, allowing unaltered specimens to be imaged in their native environments without charging effects. Furthermore, the absence of a specimen vacuum chamber provides easy access to unlimited sizes of the samples. This makes the Air-SEM imaging technique a powerful tool for real time non-destructive testing during diamond process fabrication.

Exploring optical properties is an important metrological tool for understanding diamond synthesis. There are a number of excellent works on the optical properties of diamond [14–17]. The real time study of the different spectra spanning from ultraviolet (UV) to infrared (IR) can tell us more about the doping process and how to grow diamond more efficiently.

The purpose of this work is to propose basic non-destructive characterization methods of doped diamond materials during the fabrication process. The currently investigated diamond samples include *n*-type (N), *p*-type (B) dopants and intrinsic (I), examined separately. We studied

polycrystalline diamond samples with wettability, Air-SEM, optical absorption and photoluminescence emission spectroscopy characterization methods.

2. Materials and methods

All of the investigated synthetic polycrystalline CVD diamond samples had an identical geometric polished area of 25 mm^2 (Diamond Materials Lab, Germany), where nitrogen doped iamond (5 mm × 5 mm, 300 μm thickness), intrinsic diamond (5 mm × 5 mm, 300 μm thickness) and boron doped diamond (5 mm ×5 mm, 50 μm thickness) were explored.

2.1. Optical absorption measurements

Absorption experiments were conducted using a Cary 5,000 instrument. This instrument is a high-performance UV-Vis-NIR spectrophotometer in the wavelength range of 175–3,300 nm with a Pbsmart detector.

2.2. Photoluminescence emission spectroscopy

Photoluminescence emission analysis was carried out to characterize the doping influence of the diamond bulks using the Fluorolog®-3 instrument. The experiment was conducted using a Xenon lamp light source at room temperature

2.3. Decay kinetics

Photon life time analysis was carried out to characterize the doping influence of the diamond bulks using the Deltaflex (Time Corelated Single Photon Counting) TCSPC Fluorolog Horiba. The emission detector was a TBX A single-photon detection module, (Spectral response 185–650 nm, Timing walk <250 ps FWHM). The experiment was conducted using a UV excitation Delta Nano LED at 280 nm. The Excitation pulse duration was 430.30 ns

2.4. Time-of-flight secondary ion spectroscopy

Time-of-flight secondary ion spectroscopy (ToF-SIMS) analysis was carried out to characterize the doping density of diamond bulk using a Physical Electronics TRIFT II ToF-SIMS instrument with a 15-kV Ga primary ion gun. The concentration of boron was 10^{19} cm^{-3} and of nitrogen doped diamond samples was 10^{20} cm^{-3}.

2.5. Wettability measurement

The wettability states of diamond substrates were estimated by measuring the static contact angle of sessile drops of deionized water (pH, 5.5; resistivity, 18 M cm) placed on a sample surface. Optical inspections of the wettability properties were performed using a specially designed system in our lab. The volume of liquid was kept constant (2 mL) for all contact angle measurements. The wettability investigations were carried out with an accuracy of ±1 ℃ at a temperature of 26 ± 1 ℃

and a relative humidity of 45 ± 5%. Contact angle measurements were performed 3–10 times for each sample and on different regions, in order to control surface homogeneity.

2.6. X-ray photoelectron spectroscopy measurement

X-ray Photoelectron Spectroscopy (XPS) measurements were performed in UHV (2.5×10^{-10} Torr base pressure) using a 5600 Multi-Technique System (PHI, USA). The sample was irradiated with an Al Kα monochromatic source (1486.6 eV) and the outcome electrons were analyzed by a spherical capacitor analyzer using a slit aperture of 0.8 mm. The samples were analyzed at the surface only. C1s at 285 eV was taken as an energy reference for all the measured peaks.

2.7. Air-SEM microscope measurements

In Air-SEM, electrons are emitted from an electron source in vacuum and are then collimated and focused using standard electron optics. The lower part of the column is sealed off, yet leaving a 250 μm × 250 μm area transparent to the beam electrons in the form of a thin membrane. This membrane is typically 10–15 of nanometers thick. The air gap is typically 50–100 μm thick. We used in this work back-scattered electron (BSE) and secondary electron detectors (SE). The Air-SEM resolution for this work was defined to be better than 10 nm at 30–15 keV and the contrast/brightness was a constant value for all measurements for each energy. During the measurements all samples were isolated and charged by primary beam to small negative potential.

3. Results and discussion

BSE SEM images of polished uncoated diamond samples at ambient conditions clearly show a smooth-planar surfaces with small grain boundaries of diamond (see Figure 1a). Furthermore, Figure 1b shows the same gray level (SE images were taken under the same conditions of contrast/brightness). The SE images did not show any bright or dark differences between *n*-type, intrinsic and *p*-type samples. These results imply that all samples behave identically at 30 keV. The dependence of the SE yield on primary electron beam energy is related to the penetration depth of the primary electrons and to the escape depth of the secondary electrons [18]. The penetration depth at 30 keV is higher than the escape depth of the secondary electrons, resulting in the loss of energy of many SEs before reaching the surface. In this case, the majority of emitted electrons that reach the AirSem detector surface were wide angle BSE. Therefore, with a decrease in the beam energy up to an optimum point, the penetration will be lower than the escape depth of secondary electrons, resulting in the secondary electrons escaping into air. Because of electron mean free path limitations in the AirSem system, we decided to decrease the energy to 15 keV. Figure 1c shows the SE images at 15 keV; the (B) *p*-type sample is bright and the (N) *n*-type sample is dark. The image in Figure 1c shows an increase in the contrast of (B) with 50 Hz noise. The SE detector, which is installed in the air, can detect all noises present in the room. Among the notable sources of noise is the electromagnetic wave emitted by the electrical grid, operating at a frequency of 50 Hz. Consequently, when capturing smooth samples lacking distinct edges, the detector inevitably captures the 50 Hz noise. Throughout our measurement process, we maintained the contrast and offset conditions

without any changes. However, when examining boron samples, we observed that the resulting images appeared brighter, thereby making the noise more pronounced.

According to all published research works, SE images of the dopant contrast show the *p*-type regions bright and the *n*-type regions dark. This can be explained by the energy band changing near the bulk vacuum interface and by the different built-in surface potential [8–10], the electric field produced by the charged surface states and this affects the contrast [19]. The high enhancement of the SE signal in the intrinsic sample may be attributed to electron accumulation. The explanation is based on charge generation under primary beam exposure [20].

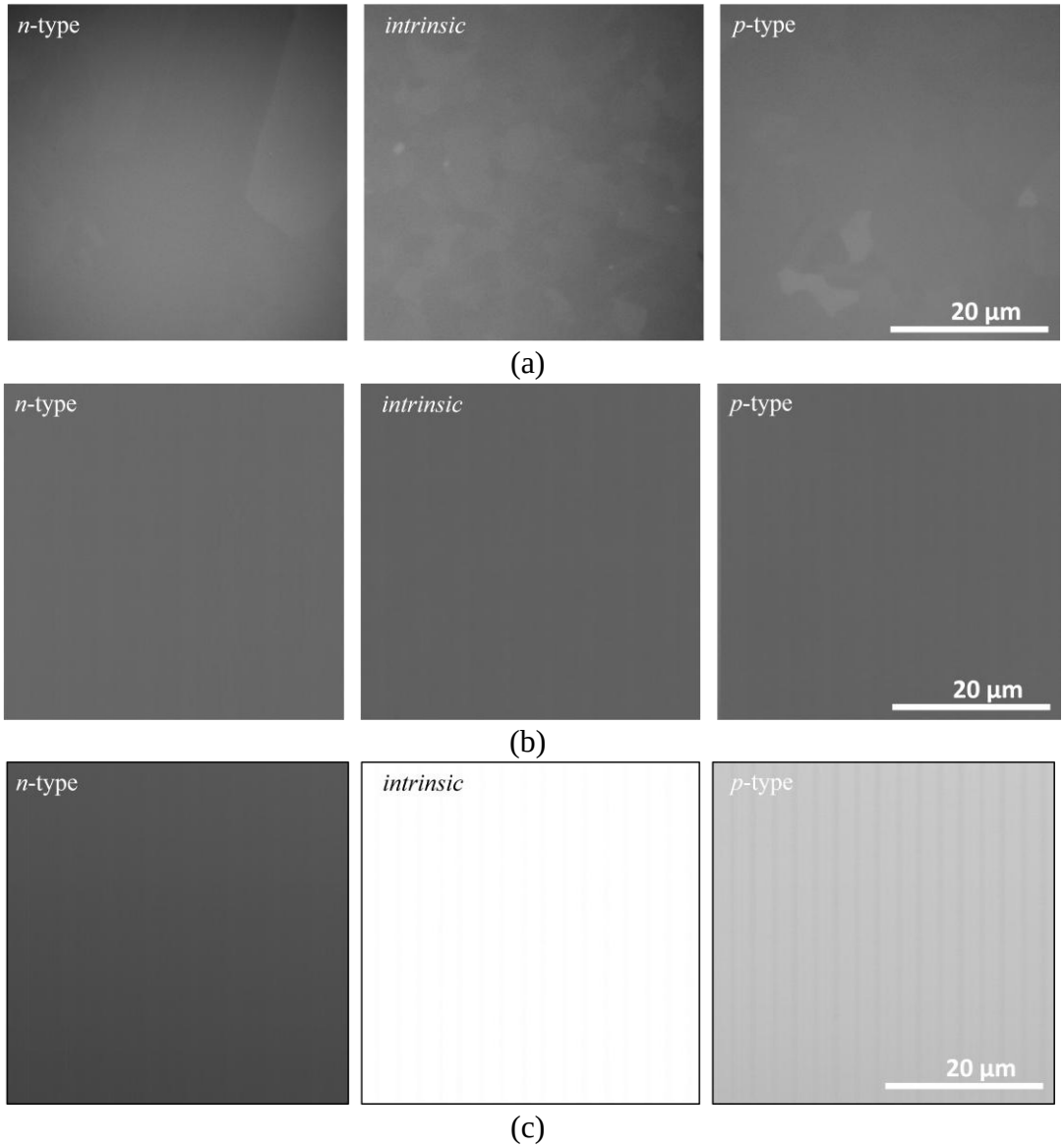

Figure 1. (a) BSE (30keV) images of the diamond sample surfaces (nitrogen doped diamond, intrinsic and boron doped diamond). (b) SE (30 keV) images of the diamond sample surfaces (nitrogen doped diamond, intrinsic and boron doped diamond). (c) SE (15 keV) images of the diamond sample surfaces (nitrogen doped diamond, intrinsic and boron doped diamond).

3.1. Wettability

In this paper, we adopt a method based on the work of Neumann [21] and the Young equation [22], and employ an approximation that makes it possible to determine the influence of doping on the surface energy of diamond doped samples.

A high wetting surface of intrinsic diamond has a surface energy that creates a strong attractive force to pull the liquid droplet down, causing it to spread out (see Figure 2). The static contact angle of a water droplet is about 60 ºon the polished CVD intrinsic diamond surface, which is close to an intrinsic WCA on a natural diamond surface. This is known as hydrophilic behavior, where the surface energy of the solid is stronger than the liquid's surface tension, causing the liquid to spread out over the homogeneous surface of the diamond [6].

Next, the water wettability behavior of the doped samples was investigated; this appears to be different (see Figure 2). The measured WCA on the boron (*p*-type) doped diamond's surface was 75 º (see Figure 2), which differs from the contact angle of 60 º for the intrinsic sample. The measured WCA on the nitrogen (*n*-type) doped diamond's surface was 50° (see Figure 2), which shows a decrease of 10 ºcompared to the intrinsic sample.

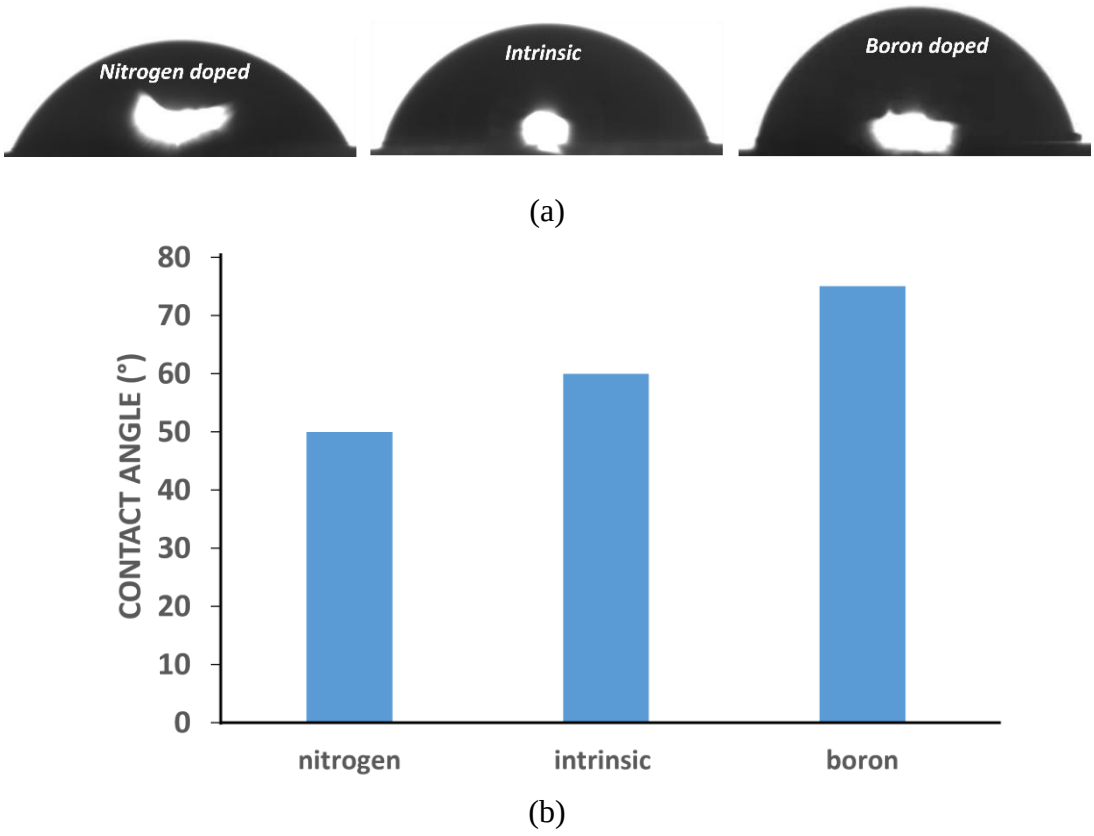

Figure 2. (a) Relationship between doping and wettability. Wettability measurement images. (b) WCA measurements of doped and undoped diamond samples.

CVD diamond samples have homogeneous solid surfaces and hydrophilic properties with negligible roughness. Based on our results, we believe that doping is the main valid factor that affects the contact angle. Thus, by using Wenzel's theory with an angle range $0\,^{\circ} < \theta < 90\,^{\circ}$[7], we can evaluate the surface tension for all diamond surfaces, based on Eq 1.

$$\cos\theta_A = r \cdot \cos\theta \tag{1}$$

where θ_A is the apparent contact angle and r is proportional to the extension of the surface area due to the roughness. Note that $r > 1$ for a rough surface, and for an ideal smooth surface $r = 1$. In this study, we consider that Eq 2

$$\cos\theta_A = \cos\theta \tag{2}$$

where θ is the contact angle corresponding to the ideal smooth diamond surface. Thus, the Young's relation corresponding to our experimental parameters to evaluate the surface tension of each diamond sample is, based on Eq 3

$$\gamma^{SV} = \gamma^{SL} + \gamma^{LV} \cdot \cos\theta \tag{3}$$

where γ are the surface tension coefficients of solid-vapor (SV), solid-liquid (SL) and liquid-vapor (LV) interfaces. However, of the four parameters of Young's equation, only γ^{LV} and θ can be readily measured. The surface tension γ^{LV} of LV at a temperature of 20 ℃ is 72.8 mN m^{-1} and the contact angle θ is measured using the experiment. To calculate the surface energy of the solid and the SL interface, two or more liquids are used in the experimental and mathematical approaches, such as the Neumann model, where the outcome strongly depends on the liquids used [23], while the solids correspond to the criteria of the Neumann model [21]. The studied solids are smooth and homogeneous, and there is no dissolution of solids nor is there any adsorption of any of the components (Wenzel behavior) from the liquid or gaseous phases by the solids. The Neumann model used to calculate the SL tension and to analyze the effect of doping on this tension and on water angle contact is, Eq 4

$$\gamma^{LV} \cdot \cos\theta = \gamma^{SV} - \gamma^{SL} \tag{4}$$

Since only γ^{LV} and θ of Young's equation can be readily measured, this equation can only provide the difference between the SV surface tension γ^{SV} and the SL interfacial tension γ^{SL}. Neumann's equation of state theory describes the contact angle (θ) of a liquid on a solid surface as, Eq 5

$$\cos\theta = -1 + 2 \cdot \sqrt{\frac{\gamma^{SV}}{\gamma^{LV}}} \cdot e^{-\beta \cdot \left(\gamma^{SV} - \gamma^{LV}\right)^2} \tag{5}$$

here $\beta = 0.0001247$ can be expressed as a universal constant [23], and the surface tension $\gamma^{LV} = 72.8\ \mathrm{mN} \cdot \mathrm{m}^{-1}$ and the contact angle θ are given in accordance with the wettability experimental results. The Neumann model is a thermodynamic approach that introduces the surface-dependent β parameter. However, according to the Neumann's experiments, differences in the β values of different materials are less than those caused by errors in contact angle measurements when using conventional methods. This is why the Neumann equation was used in order to find the SL tension surface of each diamond sample, as Eqs 6 and 7

$$\gamma^{LV} \cdot \left(\frac{cos\,\theta + 1}{2}\right)^2 = \gamma^{SV} \cdot e^{-2\beta \cdot \left(\gamma^{SV} - \gamma^{LV}\right)^2} \tag{6}$$

$$-2\beta \cdot (\gamma^{SV})^2 + 4\beta \cdot \gamma^{LV} \cdot \gamma^{SV} + \ln(\gamma^{SV}) = \ln\left[\gamma^{LV} \cdot \left(\frac{cos\,\theta + 1}{2}\right)^2\right] + 2\beta \cdot (\gamma^{LV})^2 \tag{7}$$

The SV surface tension was calculated according to the contact angle of the intrinsic diamond, $\theta = 60$ °, Eq 8:

$$\mathrm{f}\,(\gamma^{SV}) = -2.494 \cdot 10^{-4} \cdot (\gamma^{SV})^2 + 3.631 \cdot 10^{-5} \cdot \gamma^{SV} + \ln(\gamma^{SV}) + 3.195 = 0 \quad (8)$$

To solve this equation, a numerical method is necessary. First, the variations of this function were studied when γ^{SV} is strictly positive, Eq 9:

$$\mathrm{f}\,'(\gamma^{SV}) = -4.988 \cdot 10^{-4} \cdot (\gamma^{SV}) + 3.631 \cdot 10^{-5} + \frac{1}{\gamma^{SV}} = 0 \quad (9)$$

When $\gamma^{SV} \in [0\,;\,\infty]$:

$$\mathrm{f}\,'(\gamma^{SV}) = -4.988 \cdot 10^{-4} \cdot (\gamma^{SV})^2 + 3.631 \cdot 10^{-5} \cdot (\gamma^{SV}) + 1 = 0 \quad (10)$$

$$\gamma^{SV} = 44.812 \quad (11)$$

According to the signs of the derivative function (Eq 10), $f\,(\gamma^{SV})$ is increasing and continuous when $\gamma^{SV} \in [0\,;\,44.812]$, (Eq 11) and is decreasing and continuous when $\gamma^{SV} \in [44.812\,;\,\infty]$. The dichotomy method is used to solve this equation numerically (see Table 1). The growing part of this function must be analyzed in order to verify if there is a solution when $f\,(\gamma^{SV}) = 0$:

$$f\,(a_1 = 0.020) < 0 \quad (12)$$

$$f\,(b_1 = 44.812) > 0 \quad (13)$$

The function $f\,(\gamma^{SV})$ is increasing and continuous in the interval $[0\,;\,44.812]$, and $f\,(0^+)$, $f\,(44.812)$ have opposite signs. In this case, there is a unique solution when $f\,(\gamma^{SV}) = 0$ when $\gamma^{SV} \in [0\,;\,44.812]$.

In the beginning we defined the interval is [0+, 44.812], where the function resets and is continuous. We start, the initial interval $[\boldsymbol{a_n}, \boldsymbol{b_n}]$ is divided into two subintervals by finding the midpoint, $\boldsymbol{c_n}$.

$$c_n = \frac{a_n + b_n}{2} \quad (14)$$

The physical solution of the intrinsic diamond SV tension is:

$$\gamma^{SV} = 0.041 \frac{N}{m} = 41m \frac{N}{m} \quad (15)$$

The function is then evaluated at $\boldsymbol{c_n}$, and based on the sign of the function value, one of the subintervals$[\boldsymbol{a_n}, \boldsymbol{c_n}]$ or $[\boldsymbol{c_n}, \boldsymbol{b_n}]$is selected as the new interval. This process is repeated iteratively by updating the values of $\boldsymbol{a_n}$ and $\boldsymbol{b_n}$ and selecting the new midpoint until the desired level of accuracy or convergence is achieved. Repeat steps iteratively until the desired level of accuracy or convergence is achieved. This is typically determined by setting a maximum number of iterations or by checking the difference between successive values of $\boldsymbol{c_n}$, Eqs 12–15.

Calculation of SL tension leads to, Eqs 16–18:

$$\gamma^{SL} = \gamma^{SV} - \gamma^{LV} \cdot \cos\theta \quad (16)$$

$$\gamma^{SL} = 0.041 - 0.0728 \cdot \cos(60) \quad (17)$$

$$\gamma^{SL} = 4.6\, m \frac{N}{m} \quad (18)$$

The same mathematical procedure was performed for the doped-diamond samples.

All the results for the three samples have been summarized in Table 2.

Table 1. Dichotomy method.

Iteration	a_n	b_n	c_n	$f(c_n)$
1	0.020	44.812	22.416	6.180
2	0.020	1.400	0.710	2.852
3	0.020	0.710	0.365	2.187
4	0.020	0.365	0.193	1.547
5	0.020	0.193	0.107	0.956
6	0.020	0.107	0.064	0.438
7	0.020	0.064	0.042	0.025
8	0.020	0.042	0.031	−0.279
9	0.039	0.042	0.040	−0.012
10	0.040	0.042	0.041	8.1786E-04

Table 2. Results of wettability testing.

	n-type doping (Nitrogen)	Intrinsic diamond	*p*-type doping (Boron)
Water contact angle	50 º	60 º	75 º
$\gamma^{SV}\left(m\frac{N}{m}\right)$	49	41	28.8
$\gamma^{SL}\left(m\frac{N}{m}\right)$	2.3	4.6	10

3.2. Optical absorption of diamond

The optical absorption analysis of diamond samples is an important tool for elucidating the bulk properties with different diamond doping elements. In this paper, we measured three materials; intrinsic poly diamond, boron (*p*-type) doped poly diamond and nitrogen (*n*-type) doped poly diamond. SIMS was employed to analyze the composition of the diamond samples. Intrinsic carriers can be generated optically if the sample is illuminated with an energy larger than the diamond gap (5.47 eV) [16]. This corresponds to a maximum wavelength of, Eq 19:

$$\lambda = \frac{\mathrm{h} \cdot c}{E_g \cdot 1.6 \cdot 10^{-19}} = 227\ nm \tag{19}$$

where, h is Planck's constant ($h = 6.626 \times 10^{-34}$ J · s), E_g is the energy gap and c the velocity of light ($c = 3 \times 10^8$ m/s). All results are presented in Figure 3.

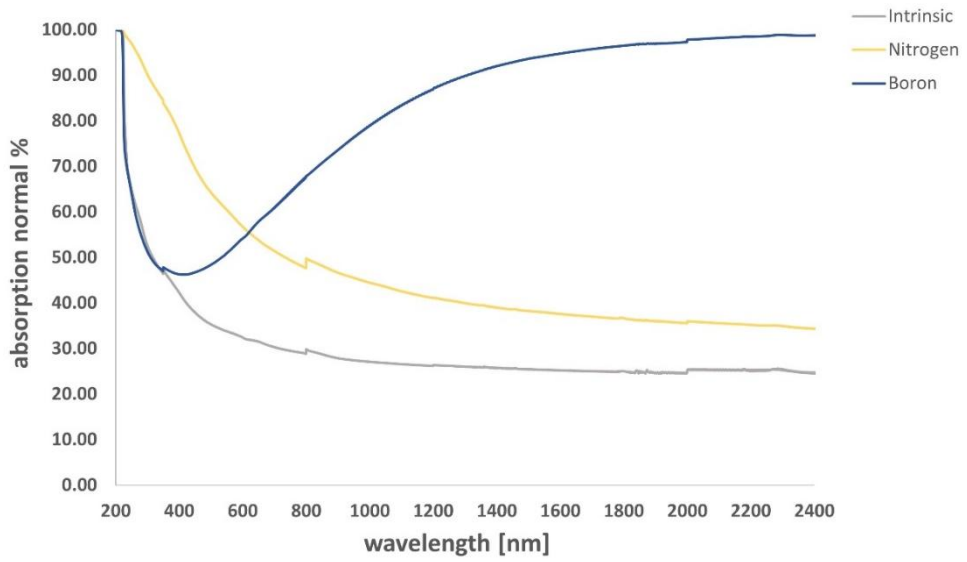

Figure 3**.** The room-temperature optical absorption of all diamond samples.

The first optical absorption experiment was carried out on the intrinsic sample. The diamond gap is indirect, and requires the excited electron to gain momentum in one of the <100> crystal directions. It can be seen that there is a moderately small rise in the absorption from around ~800 nm. Intrinsic CVD diamonds may contain a trace amount of nitrogen doping, which can be shown by examining the optical absorption characteristics. Nitrogen is a group V element, and the optical measurements indicate its energy level to be below 2 eV [16]. The main absorption occurs at 236 nm (at 5.26 eV and 0.21 eV below the indirect bandgap energy E_g), and corresponds to the excitation of an outer electron from the top of the valence band to the excitonic state just below the conduction band minimum and assisted by the phonon absorption [24].

In contrast to intrinsic diamond, nitrogen doped diamonds display a much narrower band gap. The activation energy of the nitrogen donors can be generated optically if the sample is illuminated with an energy higher than the boron gap $-E_g = 1.7\,ev$ [16]. According to Eq 19 the matching wavelength for this energy is 730 nm. It can be seen that there is a moderate rise in the absorption from around ~800 nm. It seems from Figure 3 that the UV absorption increases due to transitions of intrinsic electrons to the conduction band.

The ground state of the boron dopant acceptor center is about 0.37 eV above the valence band, and also shows hall mobility of 0.1–0.15 $m^2 \cdot V^{-1}\ S^{-1}$ [16]. This allows the doped diamond to act as a conductive material even at room temperature. According to equation 19 the matching wavelength for this energy is 3,410 nm. During the measurements, the spectrometer was limited (due to the lamp sensitivity) to a wavelength of 2,000 nm, but we can see that absorption peak continues into the IR region. The absorption in the IR spectrum corresponds to acceptor transition to excitation levels (peaks of 7.75, 4.07, 3.57 μm) [25]. Each absorption of a photon causes the excitation of one electric carrier across the bandgap, so that one obtains one additional carrier in the conduction band and one hole in the valence band.

It can be observed that in the IR spectrum that has been studied, there is full absorbance of the photons, and as the energy increases much above 0.37 eV, the photons start partially transmitting

through the sample until they absorb again in the UV spectrum (due to transitions of intrinsic electrons to the conduction band).

3.3. Photoluminescence (PL)

Photoluminescence (PL) is a widely used tool for the characterization of doping in materials. By varying the excitation photon energy, PL measurements enable the selection of different emission lines. Measurements at different excitation photon energies are then necessary to provide complete information about all elements of the bulk. PL spectra of diamond samples measured at 4.27 eV excitation are shown in Figure 4.

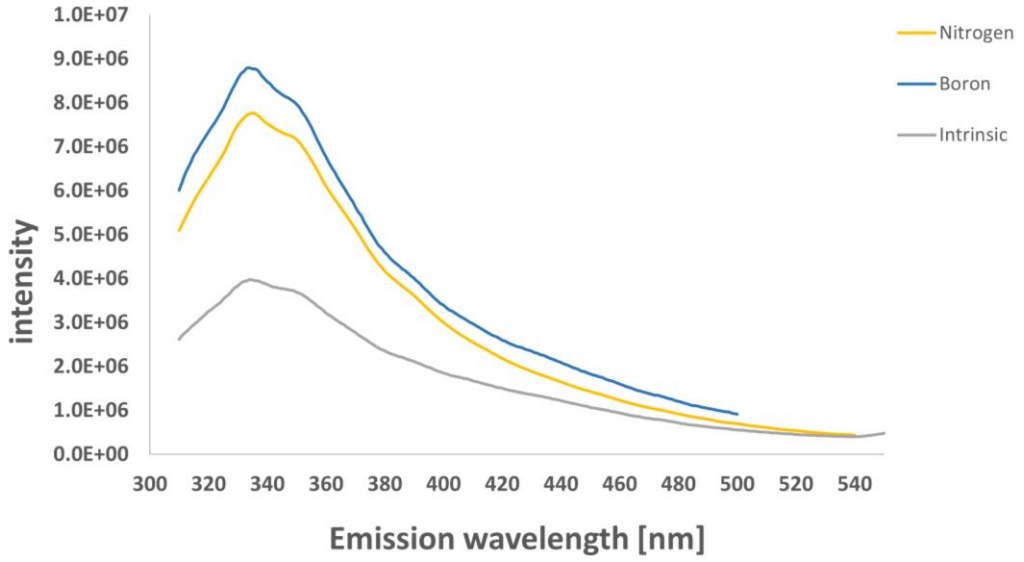

Figure 4**.** Room temperature PL spectra for diamond samples.

All samples exhibit the same related absorption. It can be observed that for an excitation wavelength of 290 nm there is a PL peak (stronger for the boron and nitrogen doped samples) at around 340 nm wavelength. During the test, the intensity of the excitation spectrum decreased with an increase in the excitation wavelength, but the shape of the spectrum remained unchanged. This confirmed the correspondence of 290 nm excitation bands with the same emission center. An absorption spectral region from 290 to 310 nm is observed in synthetic diamonds [15]. The absorption region is attributed to intrinsic nitrogen-free defects. In CVD diamond technology the impurities come from the growth system *a*nd during the etching process [26].

The PL peak at 340 nm is related to nitrogen-vacancy (NV) centers and defects [27]. The fact that the boron-doped and intrinsic samples also show this kind of peak implies that these samples might be incorporated with undesirable nitrogen-free impurities during the production process. With monochromatic (laser) excitation at wavelength of 514 nm, nitrogen-doped diamond exhibits photoluminescence of nitrogen-vacancy centers with peaks at 575 and 637 nm, which can be used as a sign of a presence of a nitrogen in diamond [27]. In our experiments these lines were not observed, possibly due to different excitation source (Xe lamp) and excitation wavelength.

3.4. Decay kinetics

The decay kinetics of the luminescence measured for all samples at 340 nm under the excitation at 280 nm is shown for nitrogen, as a representative case, in Figure 5. This decay curve shows a fast, exponential decay as a superposition of two components with decay times of 17.9 and 10.4 ns, corresponding to the emission nitrogen defect centers.

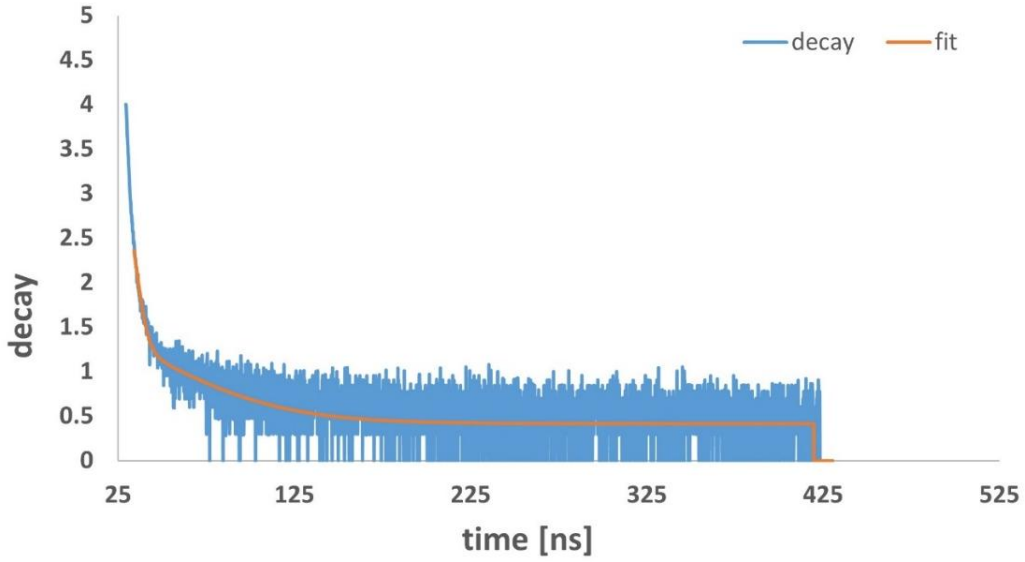

Figure 5**.** Photon lifetime in nitrogen doped diamond and 280 nm excitation wave length.

3.5. XPS characterization

The surface analysis of doped samples is important in order to elucidate the oxidation states and the surface chemical composition. Therefore, the XPS characterization for the doped diamond samples is very important in order to study the different binding energies (BEs) associated with different carbon functional groups from the C1s and O1s spectra. The main objective of this measurement is to observe the O1s/C1s atomic concentration ratio as a function of the different doping samples (see Table 3).

Table 3. Oxygen relative proportion O1s/C1s (%) contribution by peak fitting from XPS measurements.

	B	N
O1s/C1s (%)	0.5	0.666

Specifically, it seems that the oxidized surface influences the wetting angle measurements. This is in agreement with other published data and seems to confirm that diamond surface oxidation decreases the contact angle [5].

4. Conclusions

In conclusion, we used simple experimental studies to demonstrate the effectiveness of simple measurement methods for the diamond production industry. The Air-SEM shows great potential for real time product inspection. The Air-SEM without a specimen vacuum chamber allows real time product inspection and is applicable for a wide range of non-destructive line experiments, including topography and doping mapping. Furthermore, we discovered that bulk doping leads to the tunable wettability properties of diamond. The optical results, obtained from absorption and PL measurements, showed nitrogen defect centers in all samples. The XPS result showed the oxygen amount change as a function of the doping type, and displayed close agreement with the contact angle measurements.

Upon analyzing the results, we recognized the importance of investigating the correlation between doping concentration and its impact on diamond properties. To further explore this, we obtained samples with a higher doping concentration from the same manufacturer (High Doped-Diamond Materials Lab, Germany). However, upon receiving and examining these samples, we uncovered a lack of control over the high doping concentration during the production process. This lack of control introduced uncertainties and inconsistencies in the behavior of the high-doped samples after testing, which deviated from the expected behavior of diamond bulk material. In light of the challenges encountered, we emphasize the significance of future research that focuses on exploring the correlation between varying doping concentrations with experimental study methods.

Use of AI tools declaration

As the corresponding and accountable author for this publication, I would like to verify that we did not employ any AI applications linked to this research work.

Conflict of Interest

We wish to confirm that there are no known conflicts of interest associated with this publication and there has been no significant financial support for this work that could have influenced its outcome. We confirm that the manuscript has been read and approved by all named authors and that there are no other persons who satisfied the criteria for authorship but are not listed.

References

1. Wort CJH, Balmer RS (2008) Diamond as an electronic material. *Mater Today* 11: 22–28. https://doi.org/10.1016/S1369-7021(07)70349-8
2. Spear KE, Dismukes JP (1994) *Synthetic Diamond: Emerging CVD Science and Technology*, New York (N.Y.): Wiley.
3. Crawford KG, Maini I, Macdonald DA, et al. (2021) Surface transfer doping of diamond: A review. *Prog Surf Sci* 96: 100613. https://doi.org/10.1016/j.progsurf.2021.100613
4. Pinzari F, Ascarelli P, Cappelli E, et al. (2001) Wettability of HF-CVD diamond films. *Diam Relat Mater* 10: 781–785. https://doi.org/10.1016/S0925-9635(00)00609-9

5. Azevedo AF, Baldan MR, Ferreira NG (2013) Doping level influence on chemical surface of diamond electrodes. *J Phys Chem Solids* 74: 599–604. https://doi.org/10.1016/j.jpcs.2012.12.013
6. Li D, Feng X, He J, et al. (2014) Research of surface wettability of plating on the ceramic shell. *2014 15th International Conference on Electronic Packaging Technology*, 1208–1211. https://doi.org/10.1109/ICEPT.2014.6922860
7. Kubiak KJ, Wilson MCT, Mathia TG, et al. (2009) Wettability versus roughness of engineering surfaces. *Wear* 271: 523–528. https://doi.org/10.1016/j.wear.2010.03.029
8. Frank L, Hovorka M, El-Gomati MM, et al. (2020) Acquisition of the dopant contrast in semiconductors with slow electrons. *J Electron Spectrosc* 241: 146836. https://doi.org/10.1016/j.elspec.2019.03.004
9. Alugubelli SR, Fu H, Fu K, et al. (2019) Dopant profiling in p-i-n GaN structures using secondary electrons. *J Appl Phys* 126: 015704. https://doi.org/10.1063/1.5096273
10. Sealy CP, Castell MR, Wilshaw PR (2000) Mechanism for secondary electron dopant contrast in the SEM. *Microscopy* 49: 311–321. https://doi.org/10.1093/oxfordjournals.jmicro.a023811
11. Choudhary OP, Choudhary P (2017) Scanning Electron Microscope: Advantages and disadvantages in imaging components. *Int J Curr Microbiol App Sci* 6: 1877–1882. https://doi.org/10.20546/ijcmas.2017.605.207
12. Bailey GW, Dimlich RVW, McKernan S, et al. (1997) Environmental Scanning Electron Microscopy: -Advantages and disadvantages. *Microsc Microanal* 3: 381–382. https://doi.org/10.1017/S1431927600008795
13. Solomonov I, Talmi-Frank D, Milstein Y, et al. (2014) Introduction of correlative light and airSEM (TM) microscopy imaging for tissue research under ambient conditions. *Sci Rep* 4: 5987. https://doi.org/10.1038/srep05987
14. Nebel C (2020) Bulk electronic properties of diamond. arXiv preprint, arXiv:2005.03884.
15. Zaitsev AM (2021) *Optical Properties of Diamond: A Data Handbook*, Berlin, New York: Springer, xvii: 502.
16. Walker J (1979) Optical absorption and luminescence in diamond. *Rep Prog Phys* 42: 1605–1659. https://doi.org/10.1088/0034-4885/42/10/001
17. Mildren RP (2013) Intrinsic Optical Properties of Diamond. Optical Engineering of Diamond 1: 1–34. https://doi.org/10.1002/9783527648603.ch1
18. Egerton RF (2016) *Physical Principles of Electron Microscopy: An Introduction to TEM, SEM, and AEM*, Springer Cham. https://doi.org/10.1007/978-3-319-39877-8
19. Volotsenko I, Molotskii M, Barkay Z, et al. (2010) Secondary electron doping contrast: Theory based on scanning electron microscope and Kelvin probe force microscopy measurements. *J Appl Phys* 107: 014510. https://doi.org/10.1063/1.3276090
20. Grunbaum E, Barkay Z, Shapira Y, et al. (2009) Secondary electron emission contrast of quantum wells in GaAs p-i-n junctions. *Microsc Microanal* 15: 125–129. https://doi.org/10.1017/S1431927609090205
21. Li D, Neumann AW (1992) Equation of state for interfacial tensions of solid-liquid systems. *Adv Colloid Interface Sci* 39: 299–345. https://doi.org/10.1016/0001-8686(92)80064-5
22. Soleimani-gorgani A (2015) *Printing on Polymers: Fundamentals and Applications*, William Andrew.

23. Calvimontes A (2017) The measurement of the surface energy of solids using a laboratory drop tower. *npj Microgravity* 3: 25. https://doi.org/10.1038/s41526-017-0031-y
24. Clark CD, Dean PJ, Harris PV, et al. (1964) Intrinsic edge absorption in diamond. Proc R Soc London A-Math Phys Sci 277: 312–329. https://doi.org/10.1098/rspa.1964.0025
25. Aksenova AS, Altuhov AA, Ryabeva EV, et al. (2017) The investigation of boron-doped diamond absorbance spectrum. *J Phys Conf Ser* 798: 012149. https://doi.org/10.1088/1742-6596/798/1/012149
26. Mohapatra DR, Rai P, Misra A, et al. (2007) Photoluminescence study of polycrystalline and single crystal diamond. *2007 International Workshop on Physics of Semiconductor Devices*, 891–893. https://doi.org/10.1109/IWPSD.2007.4472665
27. Achard J, Jacques V, Tallaire A (2020) CVD diamond single crystals with NV centres: a review of material synthesis and technology for quantum sensing applications. *J Phys D Appl Phys* 53: 313001. https://doi.org/10.1088/1361-6463/ab81d1

AIMS Press